Transients from initial conditions in cosmological simulations

Martín Crocce,[★] Sebastián Pueblas and Román Scoccimarro
Center for Cosmology and Particle Physics, Department of Physics, New York University, New York, NY 10003, USA

ABSTRACT

We study the impact of setting initial conditions in numerical simulations using the standard procedure based on the Zel'dovich approximation (ZA). As it is well known from the perturbation theory, ZA initial conditions have incorrect second- and higher-order growth and therefore excite long-lived transients in the evolution of the statistical properties of density and velocity fields. We also study the improvement brought by using more accurate initial conditions based on second-order Lagrangian perturbation theory (2LPT). We show that 2LPT initial conditions reduce transients significantly and thus are much more appropriate for numerical simulations devoted to precision cosmology. Using controlled numerical experiments with ZA and 2LPT initial conditions, we show that simulations started at redshift $z_i = 49$ using the ZA underestimate the power spectrum in the non-linear regime by about 2, 4 and 8 per cent at $z = 0$, 1, and 3, respectively, whereas the mass function of dark matter haloes is underestimated by 5 per cent at $m = 10^{15}\,\mathrm{M}_\odot\,h^{-1}$ ($z = 0$) and 10 per cent at $m = 2 \times 10^{14}\,\mathrm{M}_\odot\,h^{-1}$ ($z = 1$). The clustering of haloes is also affected to the few per cent level at $z = 0$. These systematics effects are typically larger than statistical uncertainties in recent mass function and power spectrum fitting formulae extracted from numerical simulations. At large scales, the measured transients in higher-order correlations can be understood from first principle calculations based on perturbation theory.

Key words: methods: numerical – large-scale structure of Universe.

1 INTRODUCTION

The growth of structure in the Universe is a fundamental aspect of cosmology, and can be used to constrain the nature of primordial fluctuations and the energy contents of the Universe (e.g. dark matter and dark energy). Numerical simulations are a very important tool in making theoretical predictions of cosmological observables at small scales when fluctuations are non-linear. Fluctuations are followed from their primordial seeds through the radiation era to the matter-dominated era and current accelerating phase by using linear Boltzmann equation solvers (Peebles & Yu 1970; Bond & Efstathiou 1984; Ma & Bertschinger 1995; Seljak & Zaldarriaga 1996; Lewis, Challinor & Lasenby 2000), which are then coupled to N-body simulations to follow their non-linear evolution. This coupling takes the form of final conditions predicted from linear Boltzmann codes input as initial conditions into N-body simulations at some redshift z_i.

There are competing requirements on the best choice of z_i. One would like to start a simulation as early as possible, where perturbations are closest to their linear value, but this can be challenging from numerical reasons since one is trying to impose a small perturbation spectrum that can be overwhelmed by sources of noise such as numerical round-off error or shot noise of the particles. Also,

★E-mail: rs123@nyu.edu

when running simulations that include a baryonic component, the initial conditions simplify considerably the lower z_i is, in which case the baryons had more time to fall into the potential wells of the dark matter.

Despite the rapid progress in the development of different numerical N-body techniques for solving the non-linear growth of structure in the Universe (see e.g. Bertschinger 1998 for a review), the way initial conditions are input into these codes has essentially been the same since the first developments in cosmological simulations over 20-yr ago (Klypin & Shandarin 1983; Efstathiou et al. 1985), by using the Zel'dovich (1970) approximation (hereafter ZA).

As observations of the late Universe quickly approach per cent level accuracy, it is vital to examine to what extent theoretical predictions can accurately go from primordial fluctuations to different stages of non-linear evolution in recent epochs, e.g. redshifts $z \lesssim 3$. Studies of linear Boltzmann solvers (Seljak et al. 2003) have shown that independent codes agree to within 0.1 per cent, whereas for N-body codes the agreement, while much more difficult to quantify, is of the order of few to 10 per cent depending on the statistics and scales considered (Splinter et al. 1998; Frenk et al. 1999; Heitmann et al. 2005).

The link between Boltzmann and N-body codes, or how to set initial conditions for non-linear evolution, has been surprisingly little studied. The accuracy of the ZA has been essentially taken for granted and instead studies of initial conditions have concentrated on other (important) issues, related to how to best implement the

ZA in different situations (Bertschinger 1995; Salmon 1996; Pen 1997; Bertschinger 2001; Yoshida, Sugiyama & Hernquist 2003; Sirko 2005).

The rationale for this state of affairs seems to be that starting a simulation at 'high enough' redshift with linear perturbation theory (hereafter PT) (which the ZA is in Lagrangian space) should be safe. A rule of thumb for the choice of starting redshift often used is that the rms density fluctuations at the interparticle distance scale be of the order of 0.2. As a result, low-resolution simulations are typically started much later than high-resolution ones.

However, one of the lessons of PT (see Bernardeau et al. 2001 for a review) is that the ZA has a very limited validity, reproducing only the correct linear growth and underestimating the skewness and higher-order moments (Grinstein & Wise 1987; Juszkiewicz, Bouchet & Colombi 1993a; Juszkiewicz et al. 1993b; Bernardeau 1994; Catelan & Moscardini 1994; Baugh, Gaztañaga & Efstathiou 1995; Colombi, Bouchet & Hernquist 1995), with deviations being particularly severe for velocity field perturbations because of the ZA failure to conserve momentum.

As a result of this, starting *N*-body simulations from ZA initial conditions leads to incorrect second- and higher-order growing modes; this excites non-linear decaying modes (called *transients*) that describe how long it takes for the correct dynamics to recover the actual statistical properties of density and velocity fields (Scoccimarro 1998). This transient evolution is well understood at large scales using PT and describes the anomalous behaviour seen in measurements of higher-order moments in *N*-body simulations started from ZA initial conditions (as shown in Scoccimarro 1998 and demonstrated in much more detail below).

The importance of transients is not just of interest for studies involving higher-order moments, as we show in this paper. Underestimation of non-Gaussianity means that the tails of the probability distribution of densities and velocities will be artificially suppressed, which implies that rare events will be even more rare in a simulation that has transients. Since typically large volumes (and thus typically low resolution) are used to study rare events, the dark matter halo mass function at the high-mass end will be particularly affected by transients given that low-resolution simulations are often started later than high-resolution ones. In addition, the transient behaviour of large-scale higher-order moments implies that non-linear couplings take a significant time to develop their full strength. These are the same couplings that act at small scales and give rise to the non-linear evolution of the power spectrum, therefore transients should also affect the power spectrum at non-linear scales.

In this paper, we revisit the issue of transients from ZA initial conditions and study numerically the effects on higher-order moments, the mass function of dark matter haloes and the power spectrum. As proposed in Scoccimarro (1998), transients can be reduced significantly by using the second-order Lagrangian PT (hereafter 2LPT). This leads to correct second-order growth factors and greatly improves the behaviour of higher-order moments. Furthermore, transients in this case decay as inverse square power of the scale factor, much faster than the inverse of the scale factor in the ZA case. We study the improvement brought by using 2LPT instead of ZA in the behaviour of transients and quantify their magnitude in different statistics commonly used.

The paper is organized as follows. In Section 2, we review how transients arise and present predictions that are contrasted with simulations later. Section 3 discusses the numerical simulations we run to quantify the transients in the non-linear regime. In Section 4, we present the main results of the paper on the magnitude of transients in higher-order cumulants, power spectrum, bispectrum, mass func-

tion and bias of dark matter haloes. We summarize the results and conclude in Section 5. In Appendix A, we discuss 2LPT, and in Appendix B we derive analytically the evolution of perturbations towards a glass configuration and discuss glass initial conditions from the point of view of transients.

2 TRANSIENTS

In this section, we discuss why transients exist and how they affect the statistics of density and velocity fields at large scales, following the treatment by Scoccimarro (1998), to which we refer the reader for more details. The analytic results summarized here also give a framework to understand the measurements in simulations we discuss below at small scales. Throughout this paper, we assume Gaussian primordial fluctuations. For the most part, we assume a flat Universe with $\Omega_m = 1$ and $\Omega_\Lambda = 0$, we mention the more general case at the end of Section 2.1.

2.1 Equations of motion

The equations of motion for the evolution of dark matter can be written in a compact way by introducing the two-component 'vector'

$$\Psi_a(\boldsymbol{k}, \eta) \equiv (\delta(\boldsymbol{k}, \eta), \ -\theta(\boldsymbol{k}, \eta)/\mathcal{H}), \tag{1}$$

where the index $a = 1, 2$ selects the density or velocity components, with $\delta(\boldsymbol{k})$ being the Fourier transform of the density contrast $\delta(\boldsymbol{x}, \tau) = \rho(\boldsymbol{x})/\bar{\rho} - 1$ and similarly for the peculiar velocity divergence $\theta \equiv \nabla \cdot \boldsymbol{v}$. $\mathcal{H} \equiv \mathrm{d} \ln a/\mathrm{d}\tau$ is the conformal expansion rate with $a(\tau)$ being the cosmological scale factor and τ being the conformal time. The time variable η is defined from the scale factor by

$$\eta \equiv \ln a(\tau), \tag{2}$$

corresponding to the number of e-folds of expansion. The equations of motion in Fourier space can then be written as (we henceforth use the convention that repeated Fourier arguments are integrated over)

$$\partial_\eta \Psi_a(\boldsymbol{k}) + \Omega_{ab} \Psi_b(\boldsymbol{k}) = \gamma_{\mathrm{abc}}^{(\mathrm{s})}(\boldsymbol{k}, \boldsymbol{k}_1, \boldsymbol{k}_2) \ \Psi_b(\boldsymbol{k}_1) \ \Psi_c(\boldsymbol{k}_2), \tag{3}$$

where

$$\Omega_{ab} \equiv \begin{bmatrix} 0 & -1 \\ -3/2 & 1/2 \end{bmatrix}, \tag{4}$$

describes the linear structure of the equations of motion. In particular, the first row describes the linearized continuity equation $\partial_\eta \Psi_1 - \Psi_2 = 0$ and the second row describes linearized momentum conservation, with the two entries being the Poisson equation $[\nabla^2 \Phi = (3/2)\mathcal{H}^2 \delta]$ and the Hubble drag term, respectively. The symmetrized vertex matrix $\gamma_{\mathrm{abc}}^{(\mathrm{s})}$ describes the non-linear interactions between different Fourier modes and is given by

$$\gamma_{121}^{(\mathrm{s})}(\boldsymbol{k}, \boldsymbol{k}_1, \boldsymbol{k}_2) = \delta_{\mathrm{D}}(\boldsymbol{k} - \boldsymbol{k}_1 - \boldsymbol{k}_2) \ \frac{(\boldsymbol{k}_1 + \boldsymbol{k}_2) \cdot \boldsymbol{k}_1}{2k_1^2}, \tag{5}$$

$$\gamma_{222}^{(\mathrm{s})}(\boldsymbol{k}, \boldsymbol{k}_1, \boldsymbol{k}_2) = \delta_{\mathrm{D}}(\boldsymbol{k} - \boldsymbol{k}_1 - \boldsymbol{k}_2) \ \frac{|\boldsymbol{k}_1 + \boldsymbol{k}_2|^2 (\boldsymbol{k}_1 \cdot \boldsymbol{k}_2)}{2k_1^2 k_2^2}, \tag{6}$$

$\gamma_{abc}^{(\mathrm{s})}(\boldsymbol{k}, \boldsymbol{k}_i, \boldsymbol{k}_j) = \gamma_{acb}^{(\mathrm{s})}(\boldsymbol{k}, \boldsymbol{k}_j, \boldsymbol{k}_i)$ and γ is zero otherwise, δ_{D} denotes the Dirac delta distribution. The formal integral solution to equation (3) is given by (see Scoccimarro 2000a for a detailed derivation)

$$\Psi_a(\boldsymbol{k}, \eta) = g_{ab}(\eta) \ \phi_b(\boldsymbol{k}) + \int_0^\eta \mathrm{d}\eta' \ g_{ab}(\eta - \eta')$$
$$\times \gamma_{bcd}^{(\mathrm{s})}(\boldsymbol{k}, \boldsymbol{k}_1, \boldsymbol{k}_2) \Psi_c(\boldsymbol{k}_1, \eta') \Psi_d(\boldsymbol{k}_2, \eta'), \tag{7}$$

where $\phi_a(\boldsymbol{k}) \equiv \Psi_a(\boldsymbol{k}, \eta = 0)$ denotes the initial conditions, set when the linear growth factor $a(\tau) = 1$ and $\eta = 0$. The linear propagator $g_{ab}(\eta)$ is simply related to Ω_{ab}, and given by an inverse Laplace transform ($\eta \geqslant 0$)

$$g_{ab}(\eta) = \oint \frac{\mathrm{d}s}{2\pi\mathrm{i}}\, \mathrm{e}^{s\eta}\, (\Omega_{ab} + s\, \delta_{ab})^{-1} \tag{8}$$

which given equation (4) yields

$$g_{ab}(\eta) = \frac{\mathrm{e}^{\eta}}{5} \begin{bmatrix} 3 & 2 \\ 3 & 2 \end{bmatrix} - \frac{\mathrm{e}^{-3\eta/2}}{5} \begin{bmatrix} -2 & 2 \\ 3 & -3 \end{bmatrix}. \tag{9}$$

This describes the standard linear evolution of the density and velocity fields from their initial conditions specified by $\phi_a(\boldsymbol{k})$.

In the ZA, the Poisson equation is replaced by $\nabla^2\Phi = -(3/2)\mathcal{H}\theta$ (Munshi & Starobinsky 1994; Hui & Bertschinger 1996), and thus equation (4) is replaced by

$$\Omega_{ab}^{\mathrm{ZA}} \equiv \begin{bmatrix} 0 & -1 \\ 0 & -1 \end{bmatrix}, \tag{10}$$

which from equation (8) gives the linear propagator

$$g_{ab}^{\mathrm{ZA}}(\eta) = \mathrm{e}^{\eta} \begin{bmatrix} 0 & 1 \\ 0 & 1 \end{bmatrix} + \begin{bmatrix} 1 & -1 \\ 0 & 0 \end{bmatrix}. \tag{11}$$

The change in the linear propagator (a reflection of gravity being driven by the velocity divergence instead of density fluctuations) has important consequences, as its structure determines the generation of non-Gaussianity.

From equation (7), we can see why transients arise. For simplicity, let us assume first that the equations of motion are linear, i.e. that $\gamma_{abc} = 0$ and the second term in the right-hand side of equation (7) is zero. Then, selecting growing mode initial conditions is very simple. All we have to do is to select $\phi_a(\boldsymbol{k}) = \delta_0(\boldsymbol{k})\, u_a$, where $\delta_0(\boldsymbol{k})$ is a Gaussian random field whose power spectrum follows from a Boltzmann solver and $u_a = (1, 1)$ selects the growing mode upon contraction with g_{ab} in equation (9). Selecting the growing mode is easy since we can solve the linear evolution analytically (given by the first term in equation 7), otherwise one would generally excite the decaying mode.

In the non-linear case, we do not know an exact solution (that is the purpose of running a simulation), therefore we cannot select initial conditions in the exact (non-linear) growing mode. The best we can do is to try to use PT to select the fastest growing mode at each order in PT (2LPT achieves this to second order, and does a good job for higher orders as well). Since the initial conditions will not be in the exact growing mode, decaying modes will be excited by non-linear interactions in the second term of equation (7): these are what we call *transients*. This is analogous to what would happen in the linear case if $\phi_a(\boldsymbol{k})$ was not the eigenvector $(1, 1)$, i.e. the decaying mode in the second term of equation (9) would be excited.

In the non-linear case, the problem of transients is worse than one might think based on linear theory because transients do not go away as fast as in linear theory, where the decaying mode is suppressed by $a^{-5/2}$ compared to the growing mode. Indeed, if the ZA is used to set initial conditions, transients are only suppressed by a^{-1}, so they take a long time to decay. Using better initial conditions, such as 2LPT, leads to a^{-2} suppression, a substantial improvement.

To describe transients in a quantitative way, we expand the initial and final conditions in terms of Gaussian linearly evolved density perturbations $\delta_0(\boldsymbol{k})$,

$$\phi_a(\boldsymbol{k}) = \sum_{n=1}^{\infty} \phi_a^{(n)}(\boldsymbol{k}), \qquad \Psi_a(\boldsymbol{k}, \eta) = \sum_{n=1}^{\infty} \Psi_a^{(n)}(\boldsymbol{k}, \eta), \tag{12}$$

with

$$\phi_a^{(n)}(\boldsymbol{k}) = [\delta_{\mathrm{D}}]_n\, \mathcal{I}_a^{(n)}(\boldsymbol{k}_1, \ldots, \boldsymbol{k}_n)\, \delta_0(\boldsymbol{k}_1) \cdots \delta_0(\boldsymbol{k}_n), \tag{13}$$

$$\Psi_a^{(n)}(\boldsymbol{k}, \eta) = [\delta_{\mathrm{D}}]_n\, \mathcal{F}_a^{(n)}(\boldsymbol{k}_1, \ldots, \boldsymbol{k}_n; \eta)\, \delta_0(\boldsymbol{k}_1) \cdots \delta_0(\boldsymbol{k}_n), \tag{14}$$

where $[\delta_{\mathrm{D}}]_n \equiv \delta_{\mathrm{D}}(\boldsymbol{k} - \boldsymbol{k}_{1,\ldots,n})$ and $\boldsymbol{k}_{1,\ldots,n} \equiv \boldsymbol{k}_1 + \cdots + \boldsymbol{k}_n$. The kernels $\mathcal{I}_a^{(n)}$ describe how the initial conditions are set (at $\eta = 0$), e.g. if linear theory is used $\mathcal{I}_a^{(1)} = u_a = (1, 1)$ and $\mathcal{I}_a^{(n)} = 0$ for $n > 1$. The kernels $\mathcal{F}_a^{(n)}(\eta)$ describe how perturbations evolve after initial conditions are set, they obey the recursion relation (Scoccimarro 1998)

$$\mathcal{F}_a^{(n)}(\eta) = \sum_{m=1}^{n-1} \int_0^{\eta} \mathrm{d}s\, g_{ab}(\eta - s) \gamma_{bcd}^{(s)} \mathcal{F}_c^{(m)}(s)\, \mathcal{F}_d^{(n-m)}(s) \\ + g_{ab}(\eta)\, \mathcal{I}_b^{(n)}, \tag{15}$$

obtained by replacing equation (12) and equations (13)–(14) into equation (7). For brevity, we have suppressed the Fourier arguments. Note that $\mathcal{F}_a^{(n)}(\eta = 0) = \mathcal{I}_a^{(n)}$ as it should be, afterwards the fastest growing mode behaves as $\mathcal{F}_a^{(n)}(\eta) \sim \mathrm{e}^{n\eta}$ at each order n. Transients determine how fast one goes from initial conditions given by $\mathcal{I}_a^{(n)}$ to the regime where final conditions are in the fastest growing mode $\mathcal{F}_a^{(n)}(\eta) \sim \mathrm{e}^{n\eta}$.

If the initial conditions are not set using linear theory, the kernels $\mathcal{I}_a^{(n)}$ obey recursion relations that follow from the dynamics used to set them. For ZA initial conditions, $\mathcal{I}_a^{(n)}$ obeys

$$\mathcal{I}_a^{(n)} = \sum_{m=1}^{n-1} \int_{-\infty}^{\eta} \mathrm{d}s\, \mathrm{e}^{n(s-\eta)} g_{ab}^{\mathrm{ZA}}(\eta - s) \gamma_{bcd}^{(s)} \mathcal{I}_c^{(m)} \mathcal{I}_d^{(n-m)}, \tag{16}$$

with the condition $\mathcal{I}_a^{(1)} = (1, 1)$. This can be understood from equation (15) by using linear theory initial conditions and keeping the fastest growing mode, formally done by evolving by an infinite amount of time (from $s = -\infty$). Note that these kernels are independent of η, that is guaranteed due to the lower limit in the time integral. In the long time limit, the $\mathcal{F}_a^{(n)}(\eta)$ kernels approach $\mathcal{F}_a^{(n)}(\eta) = \mathrm{e}^{n\eta} \mathcal{H}_a^{(n)}$, where $\mathcal{H}_a^{(n)}$ obeys the recursion relation in equation (16) with the linear propagator g_{ab}^{ZA} replaced by g_{ab} (equation 9). It is easy to check that if $\mathcal{I}_a^{(n)}$ is replaced by such $\mathcal{H}_a^{(n)}$ in equation (15), then $\mathcal{F}_a^{(n)}(\eta) = \mathrm{e}^{n\eta} \mathcal{H}_a^{(n)}$ is a solution at all times, i.e. there are no transients, as expected since one is setting initial conditions exactly, i.e. in the fastest growing mode.

Although most simulations are started by initial conditions described by the kernels in equation (16) when using the ZA, some authors (Efstathiou et al. 1985; Power et al. 2003) define the velocities in a different way, by applying the ZA prescription to the *perturbed* density field after particles have been moved instead of the linear density field. In this case, it can be shown (Scoccimarro 1998) that the velocity divergence kernels are not those in the ZA, but rather they are equal to the *density* kernels in the ZA. That leads to a reduction in the time-scale of transients by a factor of about 2 (Scoccimarro 1998). We will not consider this possibility here, as the standard ZA starts are most often used in the literature, and the improvement brought by using this prescription for the velocities does not fully address the limitations of the ZA (e.g. the second-order growth is incorrect, and the transients still evolve as the inverse of the scale factor).

As an example, the second-order density kernel reads from equation (15), with $x \equiv \hat{k}_1 \cdot \hat{k}_2$,

$$\mathcal{F}_1^{(2)}(\eta) = e^{2\eta}\left[\frac{5}{7} + \frac{x}{2}\left(\frac{k_1}{k_2} + \frac{k_2}{k_1}\right) + \frac{2}{7}x^2\right] + e^{\eta}\frac{3}{10}(x^2 - 1)$$
$$+ e^{-3\eta/2}\frac{3}{35}(x^2 - 1), \tag{17}$$

which interpolates between the ZA value at $\eta = 0$ and the exact value for large η (that in between square brackets). Note that, as mentioned above, the dominant transient term is suppressed only by a single inverse power of the scale factor, so it takes a long time to disappear. If 2LPT is used to set initial conditions, the second-order kernels are reproduced exactly and there are no transients to this order. For higher-order kernels, 2LPT shows transients suppressed by inverse square powers of the scale factor (Scoccimarro 1998), and as we see below they are greatly reduced compared to the ZA case.

In making predictions that evolve all the way to $z = 0$, one must take into account the dependence on cosmological parameters neglected so far. A simple and rather accurate way of doing this is to redefine in equation (1), $-\theta(\boldsymbol{k}, \eta)/f\mathcal{H}$ as the second component, where $f \equiv \mathrm{d}\ln D_+/\mathrm{d}\ln a$ and D_+ is the growth factor with the exact cosmological dependence. When this is done, the only change in the equations of motion is $3/2 \to 3\Omega_{\mathrm{m}}/2f^2$ in equation (4), and given that $f \simeq \Omega_{\mathrm{m}}^{5/9}$ (Bouchet et al. 1995) for flat models with a cosmological constant this can be well approximated by the $\Omega_{\mathrm{m}} = 1$ value of $3/2$ since during most of the time evolution Ω_{m}/f^2 is very close to unity. This leads to the same kernels as in the $\Omega_{\mathrm{m}} = 1$ case but with the scale factor replaced everywhere by the growth factor D_+.

2.2 Statistics

We now discuss quantitatively the impact of transients on statistics of the density field at large scales. Since linear growing modes are reproduced exactly, the power spectrum at large scales is not affected by transients. The effect of transients at large scales is only felt by higher-order spectra, such as the bispectrum, or cumulants, e.g. the skewness and kurtosis. However, as these quantities characterize non-linear couplings, they are useful for understanding the results at small scales where non-linearities play a role in the power spectrum, which will then be affected by transients, as we shall see using simulations in Section 4.2.

The power spectrum $P(k)$, bispectrum $B_{123} \equiv B(k_1, k_2, k_3)$ and trispectrum T_{1234} are given by

$$\langle \delta(\boldsymbol{k})\delta(\boldsymbol{k}')\rangle = \delta_{\mathrm{D}}(\boldsymbol{k} + \boldsymbol{k}')\, P(k), \tag{18}$$

$$\langle \delta(\boldsymbol{k}_1)\delta(\boldsymbol{k}_2)\delta(\boldsymbol{k}_3)\rangle = \delta_{\mathrm{D}}(\boldsymbol{k}_{123})\, B_{123}, \tag{19}$$

$$\langle \delta(\boldsymbol{k}_1)\delta(\boldsymbol{k}_2)\delta(\boldsymbol{k}_3)\delta(\boldsymbol{k}_4)\rangle_{\mathrm{c}} = \delta_{\mathrm{D}}(\boldsymbol{k}_{1234})\, T_{1234}, \tag{20}$$

with $\boldsymbol{k}_{123} \equiv \boldsymbol{k}_1 + \boldsymbol{k}_2 + \boldsymbol{k}_3$, etc., and the subscript 'c' denotes a connected contribution, whereas the skewness S_3 and kurtosis S_4 are given by

$$S_3 = \frac{\langle\delta^3\rangle}{\langle\delta^2\rangle^2}, \qquad S_4 = \frac{\langle\delta^4\rangle_{\mathrm{c}}}{\langle\delta^2\rangle^3}. \tag{21}$$

In second-order PT, the bispectrum reads

$$B_{123} = 2\mathcal{F}_1^{(2)}(\boldsymbol{k}_1, \boldsymbol{k}_2; \eta)\, P_0(k_1)\, P_0(k_2) + \text{ cyclic}, \tag{22}$$

where P_0 denotes the power spectrum of the linear fluctuations at the initial conditions [i.e. $P(k) = a^2 P_0(k)$ in linear theory], and cyclic

permutations over $\{k_1, k_2, k_3\}$ are understood. The first three cumulants are given by

$$\langle\delta^2\rangle = \int P(k)\, W^2(kR)\, \mathrm{d}^3 k, \tag{23}$$

$$\langle\delta^3\rangle = \int B_{123}\, W_1 W_2 W_3\, \delta_{\mathrm{D}}(\boldsymbol{k}_{123})\, \mathrm{d}^3 k_1\, \mathrm{d}^3 k_2\, \mathrm{d}^3 k_3, \tag{24}$$

$$\langle\delta^4\rangle_{\mathrm{c}} = \int T_{1234}\, W_1 W_2 W_3 W_4\, \delta_{\mathrm{D}}(\boldsymbol{k}_{1234})\, \mathrm{d}^3 k_1 \cdots \mathrm{d}^3 k_4, \tag{25}$$

where $W(kR)$ represents a top hat filter in Fourier space at smoothing scale, R, and $W_i \equiv W(k_i R)$. From these expressions, it follows the skewness and kurtosis including transients (Scoccimarro 1998)

$$S_3 = \left(\frac{34}{7} - \gamma_1\right) + \frac{1}{a}(4 - \gamma_1) + \frac{1}{a}\left(\gamma_1 - \frac{26}{5}\right) + \frac{12}{35a^{7/2}}, \tag{26}$$

$$S_4 = \frac{60\,712}{1323} - \frac{62\gamma_1}{3} + \frac{7\gamma_1^3}{3} - \frac{2\gamma_2}{3} - \frac{816}{35a} + \frac{28\gamma_1}{5a} + \frac{184}{75a^2}$$
$$+ \frac{1312}{245a^{7/2}} - \frac{8\gamma_1}{5a^{7/2}} - \frac{1504}{4725a^{9/2}} + \frac{192}{1225a^7}, \tag{27}$$

where we have written the time dependence in terms of the scale factor a and

$$\gamma_p \equiv -\frac{\mathrm{d}^p \ln \sigma^2(R)}{\mathrm{d}\ln^p R}, \tag{28}$$

with $\sigma^2(R)$ being the variance of density perturbations (equation 23).

These results have also been derived more recently using a different approach based on the steepest descent method for the density probability distribution function (PDF) (Valageas 2002). In equation (26), we have explicitly written down the different contributions: the ZA contribution from initial conditions in square brackets, the exact value (reached only asymptotically as $a \to \infty$) in curly brackets, and the remaining two transient terms (which cancel the exact value when $a = 1$). If initial conditions were set using Eulerian linear theory, the term in square brackets would not be present.

As discussed above, to include the dependence of transients on cosmological parameters, we will make the replacement $a \to D_+$ in all comparisons of equations (25)–(26) with numerical simulations.

Fig. 1 evaluates equation (26) in two cases, one where ZA is used to set the initial conditions (solid), and the other when Eulerian linear theory is used (and thus $S_3 = 0$ at $a = 1$). We see that if linear theory were used, to reach the correct value of S_3 within some tolerance, it would take about four times more expansion away from the initial conditions compared to the ZA case. The difference in the two cases is purely due to the initial value of S_3, i.e. the rate of convergence to the right answer is the same (as transients go away as a^{-1} in both cases). In contrast, using 2LPT initial conditions improves the initial values of the S_p parameters dramatically over the ZA case (being exact for S_3), and also improves substantially the rate of decay of transients to a^{-2}.

Linear theory initial conditions are relevant for codes that do not use particles, e.g. in the case where baryons are described by fields in a grid instead of particles. In such cases, one must keep in mind that the magnitude of the transients we demonstrate with simulations below are very likely to be much worse, as reflected by the difference between the curves in Fig. 1.

The dependence of transients on the shape of the power spectrum, in equations (25)–(26) through γ_p, shows that transients from ZA initial conditions are somewhat reduced as the spectrum becomes
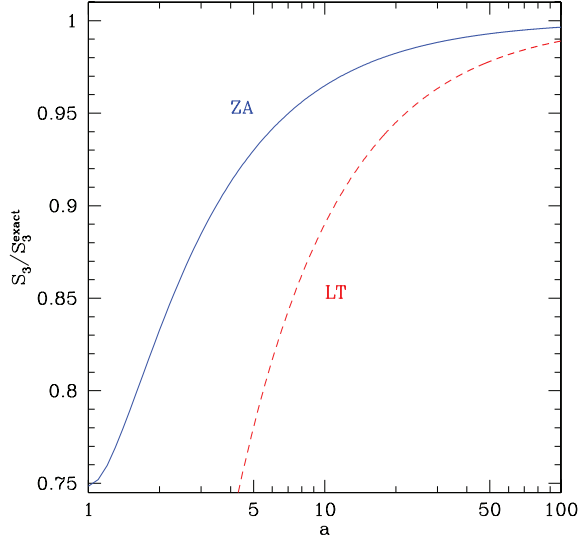
Figure 1. The skewness S_3 at $R = 10\,h^{-1}$ Mpc for ZA (solid) and Eulerian linear theory (dashed) initial conditions as a function of the expansion factor a away from initial conditions (at $a = 1$). Values are given in terms of the exact value of S_3.

steep, since the gravitational interactions are dominated by large scales and this leads to fewer deflections, i.e. more coherent displacement fields better approximated by straight-line trajectories given by the ZA. The dependence on spectrum is discussed in detail in Scoccimarro (1998). Here, we concentrate on a fixed shape given by a concordance cosmological model as discussed in the next section.

The lesson from Fig. 1 is that non-linear couplings (in this case, second order) take a significant time to develop their full strength if initial conditions are not set accurately. As expected from PT, these weaker non-linear couplings give a transient effect in the non-linear power spectrum. The effect of transients is also felt rather strongly on rare events such as the abundance of high-mass clusters, which probe the tail of the density probability distribution characterized by the S_p parameters. We demonstrate these effects below using numerical simulations.

3 SIMULATIONS

In order to study the effects of transients at small scales, we ran a set of simulations with different initial conditions (ZA and 2LPT), starting redshifts z_i, box sizes L_{box}, softening lengths (fixed in comoving coordinates) and number of time-steps as described in Table 1. All our simulations have $N_{par} = 512^3$ particles with cosmological parameters $\Omega_m = 0.27$, $\Omega_\Lambda = 0.73$, $\Omega_b = 0.046$, $h = 0.72$ and $\sigma_8(z = 0) = 0.9$, and were run using the GADGET2code (Springel 2005).

All the internal parameters to the GADGET2code used to run the different numerical experiments are also given in Table 1. In summary, we have two sets of initial conditions (ZA and 2LPT), each of them started at two different redshifts z_i with the purpose of checking the magnitude of transients. The difference between ZA and 2LPT initial conditions is explained in Appendix A in terms of Lagrangian displacements. In our implementation, particles are started from a grid and all differentiations are done in Fourier space, i.e. through $\nabla \to i\boldsymbol{k}$. Another possibility would be to start particles from a 'glass', in Appendix B we briefly discuss how to avoid inducing extra initial skewness (and thus transients) due to glass initial conditions.

A simulation without transients should have statistical properties (measured at redshift $z < z_i$) independent of z_i. Also, if generating initial conditions with the ZA was accurate enough, certainly 2LPT would be as well, since PT converges very well at high redshift. If this were the case, no appreciable difference would be seen at low redshift between ZA and 2LPT initial conditions.

However, for ZA initial conditions, we observe that statistics at low redshift *are different* than those from 2LPT initial conditions started at the same redshift (in this case $z_i = 49$), *and* we also see a clear dependence on z_i (comparing $z_i = 49$ with $z_i = 24$ simulations). Furthermore, the magnitude of transients observed at large scales agrees with the perturbative predictions presented in the previous section. In addition, the expected suppression of non-linear couplings at large scales acts at small scales in a manner consistent with what one expects physically.

How do we know that the 2LPT initial conditions simulations are correct? At large scales, we checked the numerical simulations against the PT predictions, and we see almost no dependence of the low redshift results on the starting redshift z_i. To make this latter point more obvious, we decided to present results for a very late

Table 1. Numerical simulations parameters. All our simulations have $N_{par} = 512^3$ particles with $\Omega_m = 0.27$, $\Omega_\Lambda = 0.73$, $\Omega_b = 0.046$, $h = 0.72$ and $\sigma_8(z = 0) = 0.9$, were run using GADGET2 (Springel 2005) with time integration accuracy parameters ErrTolIntAccuracy $= 0.025$, MaxRMSDisplacementFac $= 0.2$, MaxSizeTimestep $= 0.025$, and gravitational force accuracy parameters ErrTolTheta $= 0.5$, TypeOfOpeningCriterion $= 1$, ErrTolForceAcc $= 0.005$ except for the HQ runs, where more stringent parameters (ErrTolIntAccuracy $= 0.01$, MaxRMSDisplacementFac $= 0.1$, MaxSizeTimestep $= 0.01$, ErrTolTheta $= 0.2$, ErrTolForceAcc $= 0.002$) were chosen. Length units are in h^{-1} Mpc and mass units are in $10^{10}\,\mathrm{M}_\odot\,h^{-1}$.

Name	L_{box}	m_{par}	Initial conditions	z_i	$N_{realizations}$	Softening	$N_{time-steps}$
LRZA49	1024	59.94	ZA	49	8	0.2	800
LRZA24	1024	59.94	ZA	24	8	0.2	750
LR2LPT49[a]	1024	59.94	2LPT	49	8	0.2	800
LR2LPT11.5	1024	59.94	2LPT	11.5	8	0.2	650
LRsZA49	1024	59.94	ZA	49	2	0.07	1800
LRs2LPT49	1024	59.94	2LPT	49	2	0.07	1800
HRZA49	512	7.49	ZA	49	4	0.04	2200
HRZA24	512	7.49	ZA	24	4	0.04	2200
HR2LPT49[b]	512	7.49	2LPT	49	20	0.04	2200
HR2LPT11.5	512	7.49	2LPT	11.5	4	0.04	2200
HQZA49	512	7.49	ZA	49	1	0.02	6500
HQ2LPT49	512	7.49	2LPT	49	1	0.02	6500

[a]This is the reference run for $L_{box} = 1024$.
[b]This is the reference run for $L_{box} = 512$.

start, $z_i = 11.5$ (compared to our standard choice $z_i = 49$). Note that we are not advocating starting simulations at $z_i = 11.5$, this is only to prove that 2LPT initial conditions have very little transient effects. 2LPT initial conditions *do have* transient effects, although much smaller than ZA. Starting at redshift $z_i = 11.5$ makes them large enough to be measurable at $z = 3$, which allows us to estimate the magnitude of transients in our reference runs (see Section 5, for a discussion of this).

Most of the results presented here are obtained by using the 'high-resolution' runs (labelled HR in Table 1), corresponding to $L_{box} = 512\,h^{-1}$ Mpc. The 'low-resolution' (labelled LR) simulations with $L_{box} = 1024\,h^{-1}$ Mpc are used to study the high-mass tail of the dark matter halo mass function in Section 4.5. In addition, we have studied if the magnitude of transients depends on the softening length by reducing the softening length by a factor of three in the LR runs (denoted by LRs), and we have also run HR simulations with twice smaller softening length and stricter time-integration and force accuracy parameters, labelled 'high-quality' (HQ) runs in Table 1. In a test run (not included in Table 1), we saw that changing the softening length from fixed in comoving to fixed in physical coordinates had negligible impact on transients. From these sanity checks, we conclude that the magnitude of transients observed from ZA initial conditions we present below is insensitive to the choices we have made in the less time-consuming runs.

The runs with 2LPT initial conditions with $z_i = 49$ are our most accurate simulations from the point of view of transients. We denote such realizations as reference runs. In order to quantify the magnitude of transients, we measure statistics at low redshift and compare them to the same measurements in these reference runs.

4 RESULTS

4.1 Higher-order cumulants

We first start by comparing simulations for measurements of higher-order cumulants at large scales, skewness S_3 and kurtosis S_4, which are sensitive to transients and can be understood analytically using PT, as presented in Section 2.2.

Fig. 2 shows the measurement of S_3 and S_4 as a function of smoothing scale R for the reference runs HR2LPT49, after averaging over 20 realizations. The agreement at large scales with the perturbative prediction (solid lines) is excellent, better than 1 per cent for S_3 for $R > 40\,h^{-1}$ Mpc. Note that all measurements at different redshifts $z = 0, 1, 2, 3$ lie on top of each other in the large-scale limit as predicted by tree-level PT (Juszkiewicz et al. 1993a; Bernardeau 1994), and depart from it at increasingly large scales as z decreases as expected from one-loop PT (Scoccimarro & Frieman 1996; Fosalba & Gaztañaga 1998). Previous measurements in large-volume simulations such as the Hubble volume (Colombi et al. 2000) could not achieve such a clean measure of higher-order cumulants independent of z due to transients effects from $z_i = 35$ ZA initial conditions, as will become clear shortly.

Fig. 3 shows what happens with 2LPT initial conditions when the starting redshift is changed to a very late start, $z_i = 11.5$. As expected theoretically, at large scales there should be no change whatsoever in S_3 since 2LPT reproduces exactly the second-order growing modes, and that is indeed what is seen in the bottom panel. At third order, 2LPT does underestimate S_4 slightly, and that manifests in a small transient behaviour at large scales (top panel). Note that since third- and higher-order couplings are slightly smaller in 2LPT, one expects the loop corrections to S_3 and S_4 to be smaller than in the reference runs, that is indeed what is seen in both panels in Fig. 3 at small
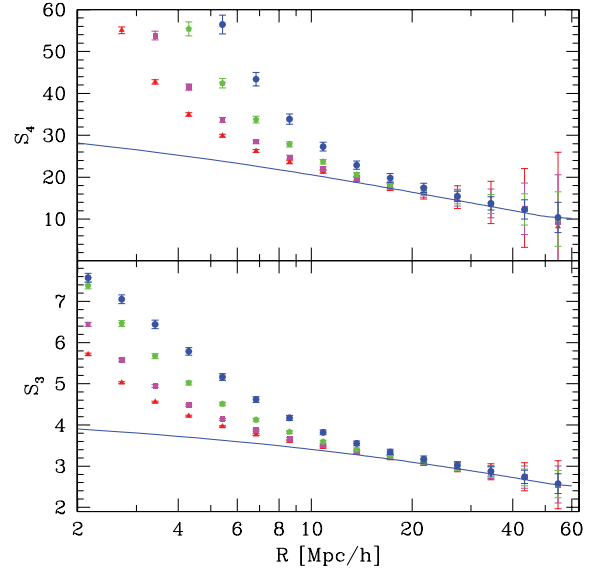

Figure 2. The skewness S_3 (bottom) and kurtosis S_4 (top) for the reference runs (2LPT $z_i = 49$) at redshifts $z = 0, 1, 2, 3$ (circles, pentagons, squares and triangles, respectively, from top to bottom in each panel). The solid lines denote tree-level PT.
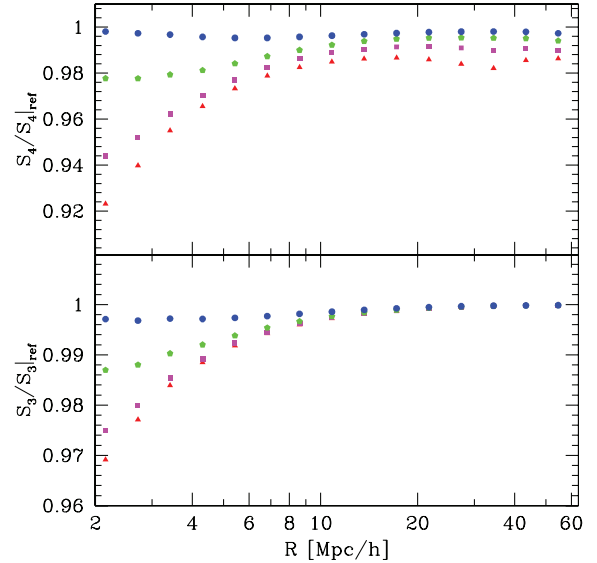

Figure 3. The skewness S_3 (bottom) and kurtosis S_4 (top) for the 2LPT $z_i = 11.5$ initial conditions compared to the reference runs ($z_i = 49$) at redshifts $z = 0, 1, 2, 3$ (circles, pentagons, squares and triangles, respectively, from top to bottom in each panel).

scales: there is a slight underestimate of the small-scale cumulants, although by the time one reaches $z = 0$, that is well under 1 per cent. Overall, the behaviour of 2LPT initial conditions is remarkably stable given the very late start, $z_i = 11.5$. In fact, we picked such a late start to make the effects visible at all at $z \lesssim 3$.

Figs 4 and 5 show the corresponding situation with ZA initial conditions for $z_i = 24, 49$, respectively. It is obvious from these figures that the ZA initial conditions runs are not stable at large scales, in particular, $z_i = 24$ and $z_i = 49$ ZA runs do not give the same results, with significant deviations at the few per cent level. These deviations are in excellent agreement with the PT predictions,
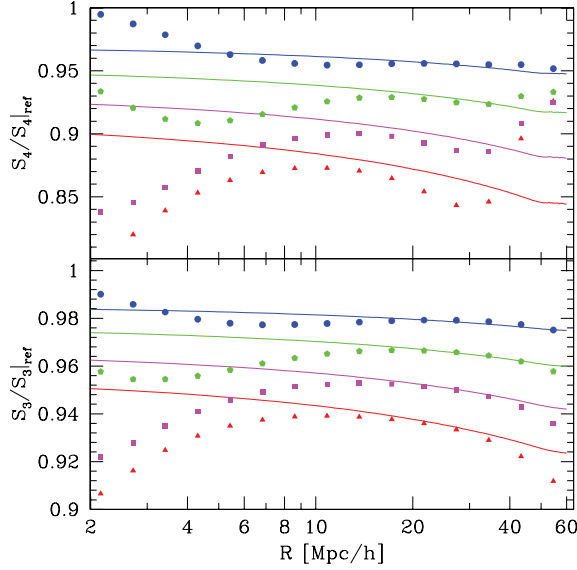
Figure 4. Same as Fig. 3 but for ZA $z_i = 24$ initial conditions. The solid lines show the predictions of the expected transient behaviour in S_3, equation (26), and S_4, equation (27).
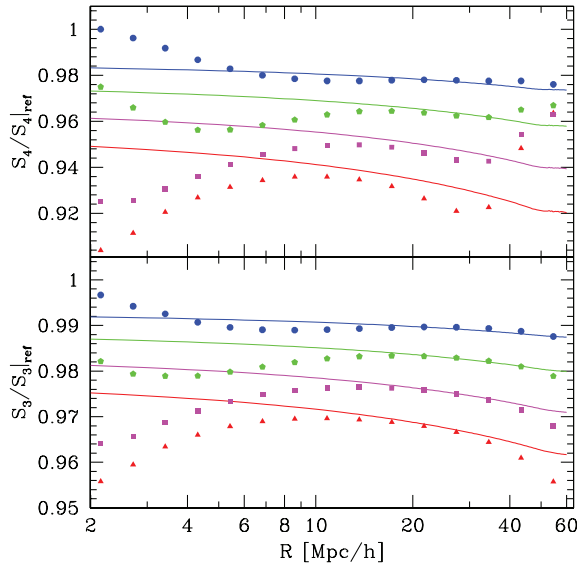

Figure 5. Same as Fig. 3 but for ZA $z_i = 49$ initial conditions. The solid lines show the predictions of the expected transient behaviour in S_3, equation (26), and S_4, equation (27).

equation (26) for the skewness (bottom panels) and equation (27) for the kurtosis (top panels). From this, we conclude that the simulations started with ZA initial conditions have transients which are well understood at large scales from first principles. Figs 4 and 5 check the PT transients predictions more accurately than done before (Scoccimarro 1998). We now discuss how these effects impact on clustering at small scales.

4.2 Power spectrum

The power spectrum is the most widely used statistic. Non-linear corrections to the power spectrum are controlled by the same non-linear couplings that determine higher-order statistics at large scales,
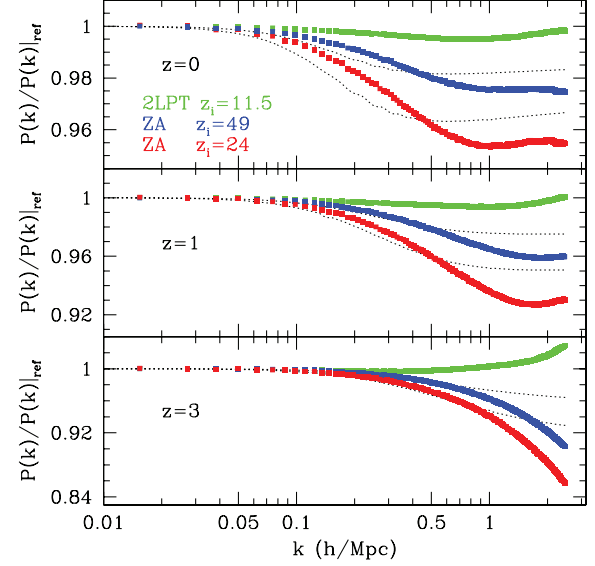
Figure 6. Power spectrum for different initial conditions (2LPT $z_i = 11.5$, ZA $z_i = 49$ and ZA $z_i = 24$, from top to bottom in each panel) compared to the reference runs at $z = 0$ (top), $z = 1$ (middle) and $z = 3$ (bottom). The dotted lines show an estimate of the transients for ZA $z_i = 49$ and ZA $z_i = 24$ from one-loop PT.

and thus we expect to see transient behaviour in the non-linear power spectrum as well.

Fig. 6 shows that this is indeed the case. First, in each panel the top line denotes the 2LPT $z_i = 11.5$ initial conditions runs, showing that in the 2LPT case there is almost no transient behaviour, as expected from the results on the S_p parameters at large scales. On the other hand, the ZA initial conditions runs show significant transient effects, up to 10 per cent at $z = 3$, which can potentially lead to serious systematic errors for precision studies of the high-redshift Universe. For example, a ZA start at $z_i = 30$ was used for the Lambda cold dark matter simulation from which the latest fitting formula for the non-linear power spectrum (Smith et al. 2003) was derived. Our reference runs show a power spectrum for $k \lesssim 2\,h\,\mathrm{Mpc}^{-1}$ that is as much as 7 per cent higher at $z = 0$ and as much as 13 per cent higher at $z = 3$ when compared to the Smith et al. (2003) fitting formula. These deviations are in reasonable agreement with the expectations based on Fig. 6. A detailed comparison of the non-linear power spectrum in our simulations to fitting formulae, one-loop PT and renormalized PT (Crocce & Scoccimarro 2006) will be discussed elsewhere.

It is also important to note that a relatively high-redshift ZA start such as $z_i = 149$, which we ran as a test, leads only to mild improvements compared to ZA $z_i = 49$ in Fig. 6, i.e. the suppression in the non-linear regime is still of the order of 1 per cent, consistent with the a^{-1} slow scaling of transients in the ZA. We have checked that these results do not depend on the accuracy of the force, time integration, and softening. For example, using the HQ runs (see Table 1) for $z_i = 49$ we obtain very similar results to those in Fig. 6, specifically within about 0.04 per cent for $z = 0, 1$ and 0.02 per cent for $z = 3$. Also, as shown in Fig. 6, the magnitude of the measured transients in the ZA $z_i = 49$ and ZA $z_i = 24$ runs are in reasonable agreement with their estimation by one-loop PT using the kernels in equation (15), particularly at high redshift where the agreement should be best.

Fig. 7 presents results in redshift space for the ZA $z_i = 49$ initial conditions runs. The combined effect of density and velocity transients leads to non-trivial behaviour. As shown by Scoccimarro
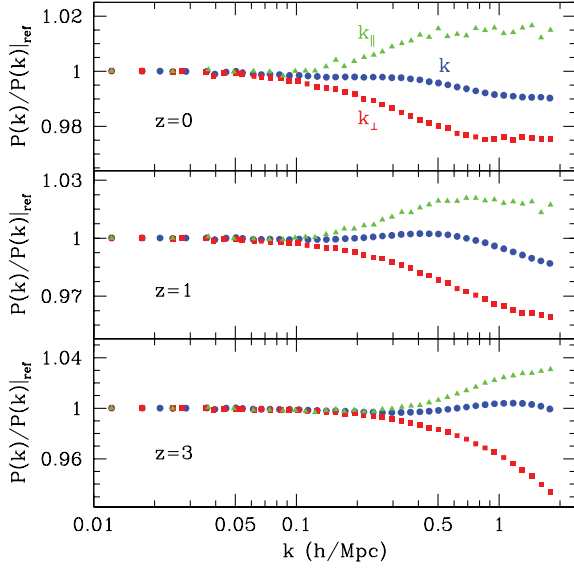
Figure 7. Redshift-space power spectrum for ZA $z_i = 49$ initial conditions compared to the reference runs at $z = 0$ (top), $z = 1$ (middle) and $z = 3$ (bottom). In each panel, we show modes parallel to the line of sight (triangles), monopole (circles) and modes perpendicular to the line of sight (squares).

Figure 8. Bispectrum for different initial conditions (2LPT $z_i = 11.5$, ZA $z_i = 49$ and ZA $z_i = 24$, from top to bottom) compared to the reference runs at $z = 0$. The symbols shown correspond to $k_1 = 0.12\,h\,\mathrm{Mpc}^{-1}$, $k_2 = 2k_1$ with θ the angle between k_1 and k_2.

(1998), transients in the velocity field are larger than in the density field. For modes parallel to the line of sight (triangles in each of the panels in Fig. 7), small-scale velocities suppress power due to velocity dispersion. Therefore, although transients in real space make the power smaller, when mapped into redshift space with velocities that are even more suppressed by transients than the density, the overall effect is to *increase* the power spectrum along the line of sight compared to the reference runs that have no transients. Since there is cancellation between density and velocity transients, the overall effect is somewhat weaker than in the real space power.

For modes perpendicular to the line of sight, on the other hand, the effect is opposite since these modes are unaffected by redshift-space distortions and show the same suppression in power seen in Fig. 6. This means that when the redshift-space power spectrum is averaged over angles with respect to the line of sight to obtain the monopole, these opposite behaviours lead to cancellation that makes the monopole less sensitive to transients (see circles in Fig. 7). However, the anisotropy of the redshift-space power spectrum is affected by transients much more than the monopole.

4.3 Bispectrum

The bispectrum is also affected by transients, and from equations (17) and (22) we see that at the largest scales where second-order Eulerian PT holds it should be affected most for triangles that are most different from elongated triangles (which correspond to $x = 1$ and show no transient behaviour). Fig. 8 shows the bispectrum at $z = 0$ for different initial conditions divided by that in the reference runs for triangles with $k_1 = 0.12\,h\,\mathrm{Mpc}^{-1}$ and $k_2 = 2k_1$ as a function of the angle θ between k_1 and k_2. From this, we see again that the 2LPT $z_i = 11.5$ initial conditions show very little ($\lesssim 0.2$ per cent) transient effects, whereas the ZA initial conditions runs show the expected transient signature, minimal at elongated triangles and maximal at isosceles triangles. These can lead to systematic errors in the determination of bias and cosmological parameters, given present expected observational errors (Sefusatti et al. 2005).
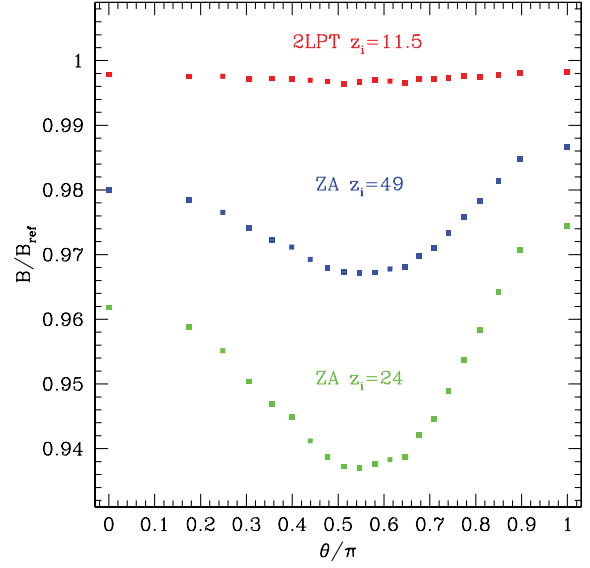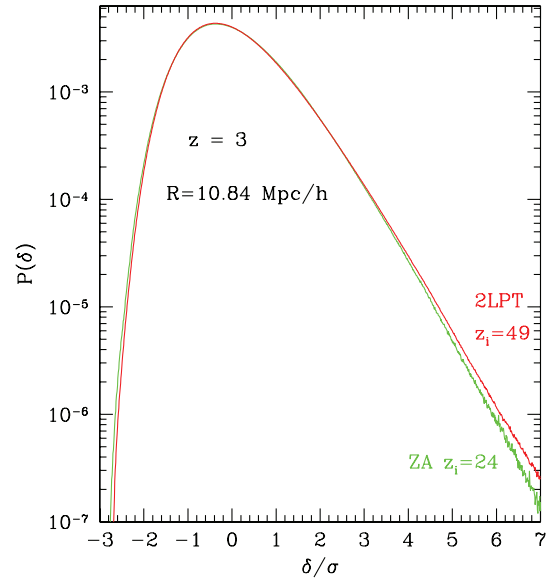

Figure 9. The PDF of the density contrast δ in units of rms value, $\sigma \equiv \langle \delta^2 \rangle^{1/2}$, for our reference run (2LPT $z_i = 49$) and ZA $z_i = 24$ initial conditions.

4.4 The PDF

The suppression of higher-order moments by transients means that the PDF of density fluctuations is also affected. Fig. 9 shows a comparison of the PDF of our reference run (2LPT $z_i = 49$) and ZA $z_i = 24$ initial conditions at redshift $z = 3$ for a smoothing scale $R = 10.84\,h^{-1}$ Mpc. Note that how the non-Gaussian features of the PDF are changed by transients: the right tail is suppressed, whereas the left cut-off is enhanced, leading to smaller skewness. Fig. 10 shows the ratio of the PDF for different initial conditions to that of the reference run, to better appreciate the differences. Although the differences at the left tail are more significant, the PDF is falling
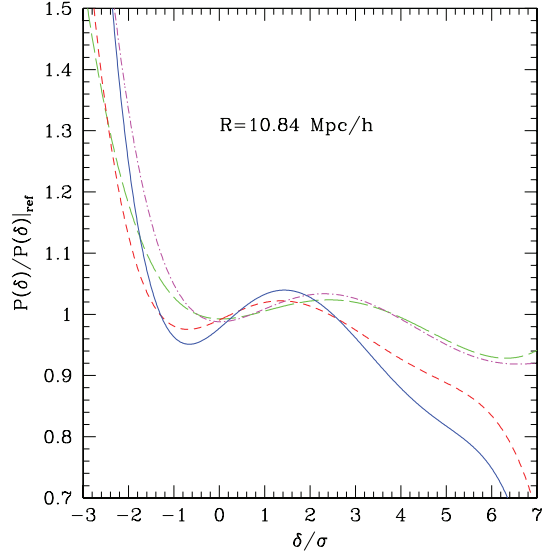
Figure 10. Ratio of PDFs for different initial conditions to our reference run. Solid lines denote ZA $z_i = 24$ at $z = 3$, dashed lines ZA $z_i = 49$ at $z = 3$, dot–dashed ZA $z_i = 24$ at $z = 0$, long dashed lines ZA $z_i = 49$ at $z = 0$.
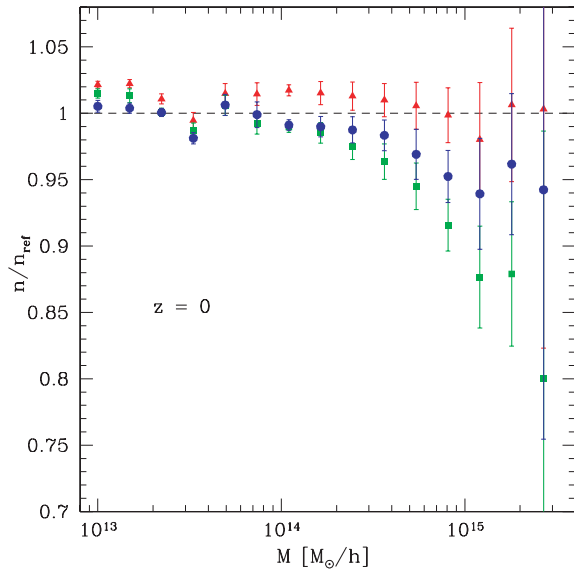

Figure 12. Mass function for ZA initial conditions with $z_i = 49$ (circles) and $z_i = 24$ (squares) compared to the reference runs at $z = 1$.

Figure 11. Mass function for different initial conditions (2LPT $z_i = 11.5$, ZA $z_i = 49$ and ZA $z_i = 24$, from top to bottom) compared to the reference runs at $z = 0$.

very steeply, thus in practice the differences seen at the right tail are more important. These correspond to high-density regions, and thus we expect these differences to impact the high-mass tail of the mass function of dark matter haloes.

4.5 The mass function

Figs 11 and 12 show the ratio of mass functions for different initial conditions to the reference runs, where the LR simulations have been used at the high-mass end to probe haloes with masses larger than $m \simeq 10^{14}$ M$_\odot$ h^{-1}. All masses have been corrected by the procedure described in Warren et al. (2006) to take into account the finite number of particles making up haloes. We use the friends-
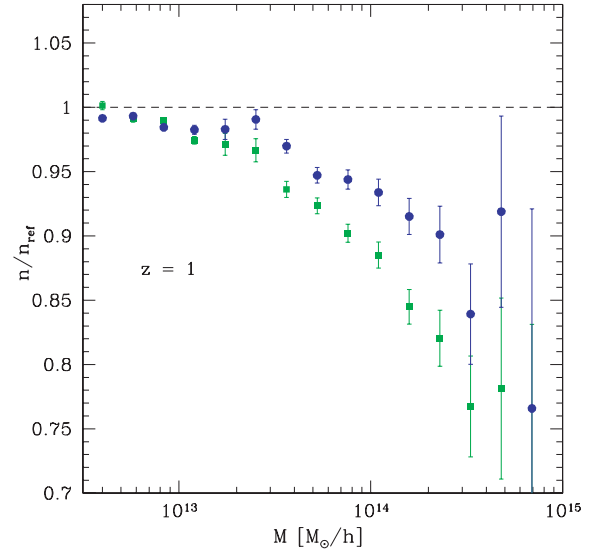
of-friends algorithm with linking length parameter equals to 0.2 to identify haloes.

The effect in the suppression of the high-mass tail is clearly seen in the simulations that were started with ZA initial conditions. The mass function in our reference runs is 15 per cent larger than the Warren et al. (2006) fitting formula for $m = 10^{15}$ h^{-1} M$_\odot$ at $z = 0$ (and thus about 30 per cent larger than the Sheth & Tormen 1999 mass function), whereas for $m < 10^{14}$ h^{-1} M$_\odot$ is consistent with the Warren et al. (2006) fit. The Jenkins et al. (2001) fit is very similar to the Warren et al. (2006) fit in the mass range covered by our simulations. These differences, in good agreement with the deviations seen in Fig. 11, are thus most likely due to transients in the simulations used to derived these fitting formulae at the high-mass end, which were started from $z_i = 24$, 35 ZA initial conditions.

Such a suppression of the mass function is clearly important for current and future observations that use the abundance of massive clusters to probe cosmology. It is also worth noting that the suppression of the mass function high-mass tail due to transients can be made worse by requiring that simulations start at a redshift z_i such that density fluctuations at the interparticle distance be a fixed number (often chosen to be about 0.2). This means that the large volume simulations that are required to probe rare events will be started later and thus will be subject to more suppression due to transients.

Using the LRs simulations with smaller softening length (see Table 1) for $z_i = 49$, we obtain very similar results to those in Fig. 11 for $z = 0$, specifically the average deviation in the eight bins with $m > 10^{14}$ M$_\odot$ h^{-1} (excluding the last one that has substantial errors) is within 0.7 per cent of that in Fig. 11. Therefore, the suppression seen in the mass function is robust to a rather large change in softening length.

Reed et al. (2003) studied the effects of the starting redshift z_i on the mass function measured at high redshifts $z \simeq 7$–15 from numerical simulations initialized with the ZA. Their statistical errors are rather large, but they do seem to see the effects we report here when comparing simulations with $z_i = 69$, 139, 279. They conclude that $z_i = 139$ is safe for measurements at $z \simeq 7$–15 and find a suppression of the high-mass tail from the Sheth & Tormen (1999) mass function which becomes stronger with z. Extrapolating our
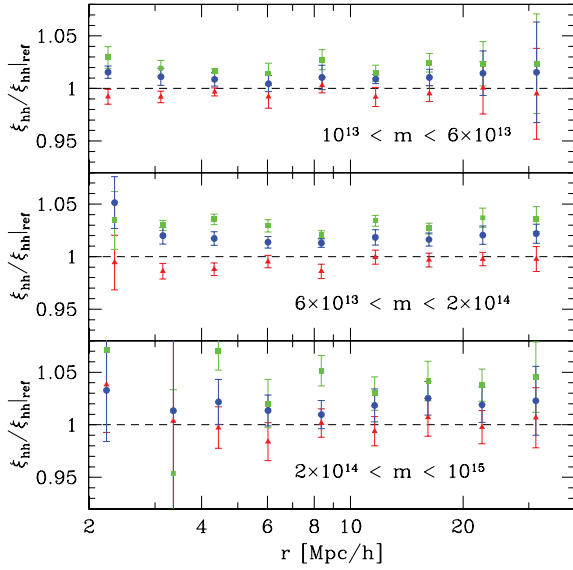
Figure 13. Ratio of halo–halo correlation functions ξ_{hh} at $z = 0$ for different initial conditions, 2LPT $z_i = 11.5$ (triangles), ZA $z_i = 49$ (circles) and ZA $z_i = 24$ (squares), compared to the reference runs at $z = 0$. The different panels correspond to three bins in halo mass as indicated (masses are in units of $h^{-1}\,M_\odot$).

results to their range, we would expect an important contribution from transients for those choices of $\{z, z_i\}$ going exactly in the same direction with increasing z. Therefore, we suggest that high-redshift studies of the high-mass tail of the mass function should be carefully checked for transients.

4.6 Halo bias

Finally, Fig. 13 shows how the clustering of dark matter haloes is affected by transients at $z = 0$. The panels show the halo–halo correlation function ξ_{hh} for different initial conditions compared to those in the reference runs, for three different mass bins. Here we have used HR simulations for the first bin in mass, and the LR simulations for the two largest mass bins. Note that as halo mass becomes larger, corresponding to rarer events, the halo bias in the simulations with more transients is *larger*. This is consistent with the fact that transients suppress the abundance of rare haloes making them more rare and thus more biased, as expected from the peak-background split.

5 SUMMARY AND CONCLUSIONS

In this paper, we considered the use of different approximations to set up initial conditions for cosmological simulations, concentrating on typical initial redshifts $z_i \simeq 50$, and studied their influence on low-redshift ($z \lesssim 3$) statistics. The standard procedure in the literature is to use the ZA, a linear solution in Lagrangian space, or even linear PT in Eulerian space (typically when simulating baryons using methods which are not based on particles).

At high redshifts ($z \sim 50$), the naive expectation is that linear perturbation theories should be accurate enough, but they are not. The reason for this is that at high redshifts non-linear corrections are relatively much more important than at low redshift because the relevant scales involved have a very steep spectrum (with the effective spectral index very close to $n_{eff} = -3$). An example of this is shown

in Fig. 9, where the density PDF smoothed on $10\,h^{-1}$ Mpc at $z = 3$ shows strong non-Gaussian features, even though naively these scales are in the linear regime (since the linear rms density fluctuation is only $\sigma = 0.25$). Modelling these non-linear corrections using the ZA leads to a significant underestimate of non-linear couplings and thus non-Gaussianity. This leads to a suppression of the density PDF tail for large densities that translates into a suppression of the high-mass tail of the mass function. The weaker non-linear couplings lead to a smaller power spectrum in the non-linear regime.

The mismatch between the approximation used to set initial conditions and the correct dynamics leads to *transients*, excitation of decaying modes that are long lived and survive until low redshift, systematically biasing low the non-linear couplings even after evolving with the correct dynamics of an *N*-body code for as much as 50–100 scale factors. Transients cannot be avoided, but they can be significantly reduced by imposing initial conditions with better approximations to the non-linear equations of motion.

More specifically, in this paper we have shown the following.

(i) The measurements of statistics at low redshift for simulations started with ZA initial conditions depend significantly on the starting redshift z_i, signalling the presence of transients.

(ii) This can be avoided to a large extent by using 2LPT initial conditions, which as we have demonstrated show very little dependence on z_i even for extremely late starts such as $z_i = 11.5$. Given that such runs show at most 1 per cent transient effects and that transients in 2LPT decay as inverse square of the scale factor, we can estimate that our reference runs with $z_i = 49$ are accurate (in terms of transients) to better than a tenth of a per cent for $z \lesssim 3$.

(iii) The simplest way to quantify transients is to follow how non-Gaussianity develops at large scales as non-linear couplings reach their full strength during the transient evolution. Our results for higher-order cumulants at large scales confirm previous PT results (Scoccimarro 1998; Valageas 2002) with much better accuracy than done before.

(iv) The small-scale behaviour of transients is consistent with the reduction of non-linear couplings observed at large scales, and we have checked it is not affected by the choice of softening length, force and time integration accuracy.

(v) The use of the ZA at $z_i = 49$ leads to suppressions in the power spectrum of the order of a few ($z = 0$) to almost 10 per cent ($z = 3$) in the non-linear regime. These results are in reasonable agreement with an estimation of transients in the power spectrum based on one-loop PT.

(vi) ZA initial conditions also lead to a suppression in the high-mass tail of the mass function of dark matter haloes. For $z_i = 24$, this suppression is about 10 per cent for $m = 10^{15}\,h^{-1}\,M_\odot$ at $z = 0$ and $m = 10^{14}\,h^{-1}\,M_\odot$ at $z = 1$. The clustering of haloes is also affected at the few per cent level.

An obvious alternative to using 2LPT initial conditions is to start with the ZA much earlier than $z_i \simeq 50$. However, in order to compete with the improvement brought by using 2LPT very high redshifts are required. For example, Fig. 6 shows that a $z_i = 11.5$ 2LPT start has approximately a 0.5 per cent transient effect on the non-linear power spectrum at $z = 0$, whereas a $z_i = 49$ ZA start has a 2.5 per cent effect. In order for the ZA to reduce the transients to the level of the 2LPT $z_i = 11.5$ start, a $z_i = 249$ ZA start would be required. Reaching the level of a 2LPT $z_i = 49$ start, corresponding to our reference runs, will require about another factor of 16 in redshift (given that transients scale as a^{-2} in 2LPT compared to a^{-1} in the ZA). Other issues make starting simulations at very high redshifts more challenging, e.g. depending on the *N*-body code algorithm, numerical

errors may be more difficult to avoid at very high redshifts where perturbations are so small, and they can accumulate as evolution is pushed forward for a longer time. In addition, initial conditions for baryons at such high redshifts must be carefully included as they are still falling into dark matter potential wells.

Although we have not studied this in any detail, simulations started with linear theory instead of the ZA are expected to be much more significantly affected by transients, e.g. a simulation started with linear theory at $z_i = 49$ should be roughly equivalent to one started with the ZA at $z = 11.5$ (see Fig. 1). Note that linear theory initial conditions are often used in codes that rely on grid methods with gas dynamics solvers. We expect such methods to show differences with e.g. smoothed particle hydrodynamics methods that use ZA initial conditions. When the dynamical variables are densities and velocities in a mesh (instead of information carried by particles), a way to reduce transients would be to use higher-order Eulerian PT.

While in this paper we have concentrated on statistics of the dark matter density perturbations, it would be interesting to know how much do transients affect other high-redshift probes, where transients are most likely to play an important role. In this regard, the most pressing aspect would be to check the impact of transients in the Lyman α forest power spectrum, because of the high accuracy demanded from simulations to obtain cosmological constraints from current data sets (Seljak, Slozar & McDonald 2006; Viel, Haehnelt & Lewis 2006).

The use of better initial conditions should be a useful tool in reaching future goals of simulating the non-linear power spectrum to an accuracy of better than 1 per cent needed for the next generation of weak gravitational lensing surveys (Huterer & Takada 2005).

The code we used to generate ZA and 2LPT initial conditions in this paper is publicly available at http://cosmo.nyu.edu/roman/2LPT.

ACKNOWLEDGMENTS

REFERENCES

Baugh C. M., Gaztañaga E., Efstathiou G., 1995, MNRAS, 274, 1049
Bernardeau F., 1994, ApJ, 433, 1
Bernardeau F., Colombi S., Gaztañaga E., Scoccimarro R., 2001, Phys. Rep., 367, 1
Bertschinger E., 1995, preprint (astro-ph/9506070)
Bertschinger E., 1998, ARA&A, 36, 599
Bertschinger E., 2001, ApJS, 137, 1
Bond J. R., Efstathiou G., 1984, ApJ, 285, L45
Bouchet F. R., Colombi S., Hivon E., Juszkiewicz R., 1995, A&A, 296, 575
Buchert T., 1994, MNRAS, 267, 811
Buchert T., Melott A. L., Weiss A. G., 1994, A&A, 288, 349
Carlberg R. G., Couchman H. M. P., 1989, ApJ, 340, 47
Catelan P., 1995, MNRAS, 276, 115
Catelan P., Moscardini L., 1994, ApJ, 426, 14
Colombi S., Bouchet F. R., Hernquist L., 1996, ApJ, 465, 14
Colombi S., Szapudi I., Jenkins A., Colberg J., 2000, MNRAS, 313, 711
Couchman H. M. P., Thomas P. A., Pearce F. R., 1995, ApJ, 452, 797
Crocce M., Scoccimarro R., 2006, Phys. Rev. D, 73, 063519
Efstathiou G., Davis M., Frenk C. S., White S. D. M., 1985, ApJS, 57, 241
Fosalba P., Gaztañaga E., 1998, MNRAS, 301, 503
Frenk C. S. et al., 1999, ApJ, 525, 554
Grinstein B., Wise M., 1987, ApJ, 320, 448
Heitmann K., Ricker P. M., Warren M. S., Habib S., 2005, ApJS, 160, 28
Hui L., Bertschinger E., 1996, ApJ, 471, 1
Huterer D., Takada M., 2005, Astropart. Phys., 23, 369
Jenkins A., Frenk C. S., White S. D. M., Colberg J. M., Cole S., Evrard A. E., Couchman H. M. P., Yoshida N., 2001, MNRAS, 321, 372
Juszkiewicz R., Bouchet F. R., Colombi S., 1993a, ApJ, 412, L9
Juszkiewicz R., Weinberg D. H., Amsterdamski P., Chodorowski M., Bouchet F. R., 1993b, ApJ, 442, 39
Klypin A. A., Shandarin S. F., 1983, MNRAS, 204, 891
Lewis A., Challinor A., Lasenby A., 2000, ApJ, 538, 473
Ma C.-P., Bertschinger E., 1995, ApJ, 455, 7
Munshi D., Starobinsky A. A., 1994, ApJ, 428, 433
Peebles P. J. E., Yu J. T., 1970, ApJ, 162, 815
Pen U.-L., 1997, ApJ, 490, L127
Power C., Navarro J. F., Jenkins A., Frenk C. S., White S. D. M., Springel V., Stadel J., Quinn T., 2003, MNRAS, 338, 14
Reed D., Gardner J., Quinn T., Stadel J., Fardal M., Lake G., Governato F., 2003, MNRAS, 346, 565
Salmon J., 1996, ApJ, 460, 59
Scoccimarro R., 1998, MNRAS, 299, 1097
Scoccimarro R., 2000a, Ann. New York Acad. Sci., 927, 13
Scoccimarro R., 2000b, ApJ, 544, 597
Scoccimarro R., Frieman J. A., 1996, ApJS, 105, 37
Sefusatti E., Crocce M., Pueblas S., Scoccimarro R., 2006, Phys. Rev. D, 74, 023522
Seljak U., Zaldarriaga M., 1996, ApJ, 469, 437
Seljak U., Sugiyama N., White M., Zaldarriaga M., 2003, Phys. Rev. D, 68, 083507
Seljak U., Slozar A., McDonald P., 2006, preprint (astro-ph/0604335)
Sheth R. K., Tormen G., 1999, MNRAS, 308, 119
Sirko E., 2005, ApJ, 634, 728
Smith R. E. et al., 2003, MNRAS, 341, 1311
Splinter R. J., Melott A. L., Shandarin S. F., Suto Y., 1998, ApJ, 497, 38
Springel V., 2005, MNRAS, 364, 1105
Valageas P., 2002, A&A, 385, 761
Viel M., Haehnelt M. G., Lewis A., 2006, MNRAS, 370, 51
Warrren M. S., Abazajian K., Holz D. E., Teodoro L., 2006, ApJ, 646, 881
White S. D. M., 1996, in Schaefer R., Silk J., Spiro M., Zinn-Justin J., eds, Cosmology and Large-Scale Structure. Elsevier, Amsterdam
Yoshida N., Sugiyama N., Hernquist L., 2003, MNRAS, 344, 481
Zel'dovich Ya. B., 1970, A&A, 5, 84

APPENDIX A: SECOND-ORDER LAGRANGIAN PERTURBATION THEORY

Here, we present the basics of 2LPT, we refer the reader to the literature (Buchert 1994; Buchert, Melott & Weiss 1994; Bouchet et al. 1995; Catelan 1995; Scoccimarro 2000b) for more information. A detailed step by step implementation of 2LPT initial conditions for numerical simulations is presented in appendix D2 of Scoccimarro (1998). Here we assume $\Omega_m = 1$ and $\Omega_\Lambda = 0$. For precision work, one must take into account the cosmological dependence, including radiation as well.

In Lagrangian dynamics, particle positions are described by a displacement field Ψ so that

$$x = q + \Psi, \tag{A1}$$

where particle trajectories obey the equation of motion

$$\frac{d^2\boldsymbol{x}}{d\tau^2} + \mathcal{H}(\tau)\frac{d\boldsymbol{x}}{d\tau} = -\nabla\Phi, \tag{A2}$$

where Φ is the gravitational potential. This leads to the following equation of motion for the displacement field

$$J(\boldsymbol{q},\tau)\nabla\cdot\left[\frac{d^2\boldsymbol{x}}{d\tau^2} + \mathcal{H}(\tau)\frac{d\boldsymbol{x}}{d\tau}\right] = \frac{3}{2}\mathcal{H}^2(J-1), \tag{A3}$$

where we have used the Poisson equation and $1 + \delta(\boldsymbol{x}) = 1/J$, where J is the Jacobian of the mapping,

$$J(\boldsymbol{q},\tau) = \mathrm{Det}(\delta_{ij} + \Psi_{i,j}), \tag{A4}$$

and $\Psi_{i,j} \equiv \partial\Psi_i/\partial q_j$.

Solving equation (A3) perturbatively leads to positions and velocities,

$$\boldsymbol{x} = \boldsymbol{q} - a\,\nabla_{\boldsymbol{q}}\phi^{(1)} - \frac{3}{7}a^2\,\nabla_{\boldsymbol{q}}\phi^{(2)}, \tag{A5}$$

$$\boldsymbol{v} = -a\,H\,\nabla_{\boldsymbol{q}}\phi^{(1)} - \frac{6}{7}a^2\,H\,\nabla_{\boldsymbol{q}}\phi^{(2)}, \tag{A6}$$

where the potentials satisfy the Poisson equations (Buchert et al. 1994)

$$\nabla_{\boldsymbol{q}}^2\phi^{(1)}(\boldsymbol{q}) = \delta(\boldsymbol{q}) \tag{A7}$$

$$\nabla_{\boldsymbol{q}}^2\phi^{(2)}(\boldsymbol{q}) = \sum_{i>j}\left\{\phi_{ii}^{(1)}(\boldsymbol{q})\phi_{jj}^{(1)}(\boldsymbol{q}) - \left[\phi_{ij}^{(1)}(\boldsymbol{q})\right]^2\right\}. \tag{A8}$$

Setting $\phi^{(2)} = 0$ in equations (A5)–(A6) leads to the ZA.

Going beyond 2LPT to third order (3LPT) becomes more costly due to the need to solve three additional Poisson equations (Buchert et al. 1994; Catelan 1995), and the improvement in higher-order statistics is modest (Scoccimarro 2000b), leading to an improvement by only a factor of 2 in the scale factor needed to suppress transients (Scoccimarro 1998), whereas going from ZA to 2LPT the improvement is more than one order of magnitude. However, 3LPT does provide a better behaviour in underdense regions (Bouchet et al. 1995), and may be worth considering for studies sensitive to the statistical properties of voids.

APPENDIX B: ON GLASS INITIAL CONDITIONS

In this paper, our numerical simulations were started from a grid. An alternative to a grid start is to displace particles from a configuration known in the literature as a glass, which is obtained starting from a Poisson distribution and running an *N*-body code with the sign of the acceleration reversed (Carlberg & Couchman 1989; Baugh, Gaztañaga & Efstathiou 1995; Couchman, Thomas & Pearce 1995; White 1996; Smith et al. 2003).

In this appendix, we derive analytically how perturbations evolve towards a glass, and what steps must be taken to avoid exacerbating the problem of transients. Reversing accelerations means that the equations of motion are still given by equation (3) but with

$$\Omega_{ab} \equiv \begin{bmatrix} 0 & -1 \\ 3/2 & 1/2 \end{bmatrix}, \tag{B1}$$

instead of equation (4). As a result the linear propagator, equation (8), reads
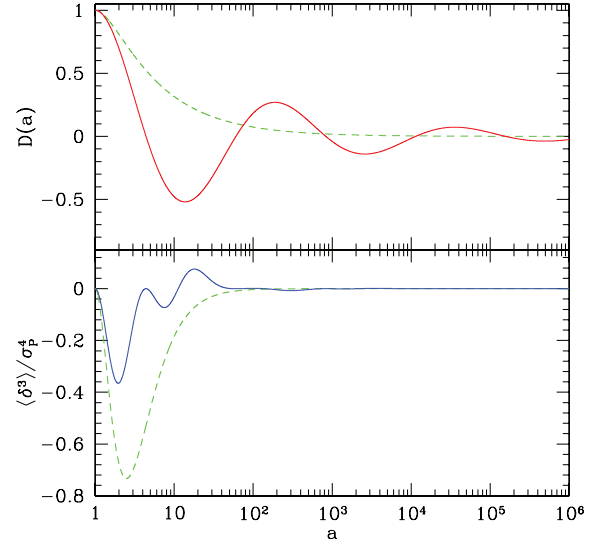

Figure B1. Evolution of perturbations towards a glass. The top panel shows the growth factor *D* as a function of scale factor *a* for standard procedure (solid) and extra-damped procedure with $\nu = 3$ (dashed). The bottom panel shows the corresponding behaviour of the third moment in terms of its Poisson value.

$$g_{ab}(\eta) = e^{-\eta/4}\left\{\cos\left(\frac{\sqrt{23}}{4}\eta\right)\begin{bmatrix} 1 & 0 \\ 0 & 1 \end{bmatrix}\right.$$
$$\left. + \frac{1}{\sqrt{23}}\sin\left(\frac{\sqrt{23}}{4}\eta\right)\begin{bmatrix} 1 & 4 \\ -6 & -1 \end{bmatrix}\right\}, \tag{B2}$$

instead of equation (9). The 'growth' factor *D* for density perturbations can be obtained by specifying how initial conditions are set before evolving towards a glass. Assuming the common choice of zero initial velocities, we have $D = g_{1b}\cdot(1,0)$ and then

$$D = \frac{1}{a^{1/4}}\left[\cos\left(\frac{\sqrt{23}}{4}\ln a\right) + \frac{1}{\sqrt{23}}\sin\left(\frac{\sqrt{23}}{4}\ln a\right)\right], \tag{B3}$$

where we have switched to the scale factor as a time variable (recall $\eta = \ln a$). Therefore, both eigenmodes contribute an overall decaying factor of $a^{-1/4}$ with oscillations of opposite phase. The top panel in Fig. B1 shows equation (B3) as a function of *a* (solid), showing that the decay of perturbations due to repulsive gravity is very slow. These damped oscillations explain the behaviour seen in fig. A2 in Baugh et al. (1995).

Using equation (15) with the propagator in equation (B2) and Gaussian Poisson initial conditions, we can derive the behaviour of the third moment as evolution proceeds towards a glass

$$\langle\delta^3\rangle_{\mathrm{glass}} = -\frac{3D^2}{299\sqrt{a}}\left[52 + (23a^{1/4} - 75)\cos\left(\frac{\sqrt{23}}{4}\ln a\right)\right.$$
$$\left. + \sqrt{23}(17a^{1/4} - 9)\sin\left(\frac{\sqrt{23}}{4}\ln a\right)\right]\sigma_{\mathrm{P}}^4, \tag{B4}$$

where σ_{P}^2 denotes the initial Poisson variance. This result is shown as a function of *a* in the bottom panel in Fig. B1 (solid). Note that (mostly negative) skewness is developed as evolution to the glass takes place, therefore although the amplitude of perturbations mostly decreases as things evolve to a glass, skewness is generated. Unless one evolves by many ($\gtrsim 10^2$) scale factors this can potentially enhance the problem of transients. The reason is that if the glass itself has negative skewness, this adds to the incorrect skewness that initial

conditions may have, as we now discuss. This issue does not arise for grid initial conditions.

Particles are displaced from their glass positions $\boldsymbol{q}$ by the displacement vector Ψ so that their positions are given by equation (A1), and the induced density perturbations then obey

$$[1 + \delta(\boldsymbol{q})]\, \mathrm{d}^3 q = [1 + \delta(\boldsymbol{x})]\, \mathrm{d}^3 x, \tag{B5}$$

where $\delta(\boldsymbol{q})$ are the density perturbations due to the distribution of starting positions. These vanish for a grid below the Nyquist frequency, but are non-zero for a glass. Then, linearizing, the total perturbation imposed on a set of particles is

$$\delta(\boldsymbol{x}) = \left(\frac{1}{J} - 1\right) + \delta(\boldsymbol{q}) \equiv \delta_{\mathrm{ic}}(\boldsymbol{x}) + \delta_{\mathrm{glass}}(\boldsymbol{x}), \tag{B6}$$

where the first term is the standard initial condition perturbation generated by the displacement field, with J given by equation (A4), and the second term is the glass perturbation, the outcome of the process described by equations (B2)–(B4). Since the two perturbations are independent, requiring that the glass skewness is negligible (and thus has no impact on transients) means to require it to be small compared to the Poisson noise of the particles (which typically is smaller than the physical perturbations δ_{ic} imposed by the initial conditions). Then one must simply require

$$\langle \delta^3 \rangle_{\mathrm{glass}} \ll \sigma_{\mathrm{P}}^4, \tag{B7}$$

which according to Fig. B1 requires $a \gtrsim 10^2$ in the evolution towards a glass.

In the desire for faster convergence towards a glass, the Hubble drag term in the equations of motion is sometimes increased to avoid oscillations (Couchman et al. 1995). Making such a modification in equation (B1) to allow for a generic drag of magnitude ν gives

$$\Omega_{ab} \equiv \begin{bmatrix} 0 & -1 \\ 3/2 & \nu \end{bmatrix}, \tag{B8}$$

which leads to propagator eigenmodes time dependence as $\mathrm{e}^{w_{\pm}\eta}$ with $2\, w_{\pm} = -\nu \pm \sqrt{\nu^2 - 6}$, and thus the requirement of no oscillations in approaching a glass gives $\nu^2 \geqslant 6$. Taking $\nu = 3$ as an example, we obtain the growth factor and third moment as before, shown in Fig. B1 as dashed lines. We see from this that although the convergence to a glass is improved in the growth factor sense, the generation of skewness is more significant, and therefore one must wait roughly the same as with $\nu = 1/2$ to have negligible impact.

Summarizing, generating a glass with an overall expansion factor by $a \gtrsim 10^2$ should be a safe configuration of points for starting cosmological simulations.

This paper has been typeset from a TEX/LATEX file prepared by the author.